SMiRT-25
Charlotte, NC, USA, August 4-9, 2019
Division I – Mechanics of Materials

POTENTIALS AND ISSUES OF ADDITIVE MANUFACTURED COMPONENTS FOR NUCLEAR POWER PLANTS

Axel Schulz[1], Torsten Fischer[2], Martin Beckert[3], Bernd Kuhn[4] and Ralf Trieglaff[5]

[1]Senior engineer, TUV NORD, Germany (aschulz@tuev-nord.de)
[2]PhD, scientific assistant, Research Center Juelich, Germany
[3]Senior engineer, TUV NORD, Germany
[4]PhD, scientific adviser, Research Center Juelich, Germany
[5]Technical adviser, TUV NORD, Germany

ABSTRACT

For the use of additively manufactured components in nuclear installations, it has to be ensured that the strict quality requirements of the codes and standards are met, regardless of the type of manufacturing process.

Activities with respect to quality control of additive components are currently focused on a sensor-based process monitoring and test methods for the subsequent quality assessment of the material structure. Intensive work is being done on analyses to determine the manufacturing quality using the process and test data.

The results of material investigations are presented for an example of a test component and for additional material samples required for the design approval process. It will be shown how the material characteristics affect the strength calculations for the design approval process.

It will also be discussed how to reduce the effort of quality control within the scope of the design approval, if special alloys tailored for the additive manufacturing process are used.

As an example a ferritic, Laves phase strengthened, high chromium steel is referenced that could be used in the new concepts for higher temperature nuclear reactors. It is demonstrated that these steels do retard both crack initiation and propagation. This can increase fatigue resistance and safety.

INTRODUCTION

TUV NORD has carried out a first research project Schulz et al. (2018) in the field of additive manufacturing of metallic materials using the laser sintering process.

As part of this projects, experience was gained in material behavior, the performance of test methods was assessed, and computational evaluation approaches for additively manufactured components were examined and adapted with regard to their applicability.

In the first step of the project, a component design was developed and two test components were manufactured simultaneously. The final structure of the test components (drawing and CAD model) and the associated FEA model are shown in figure 1.

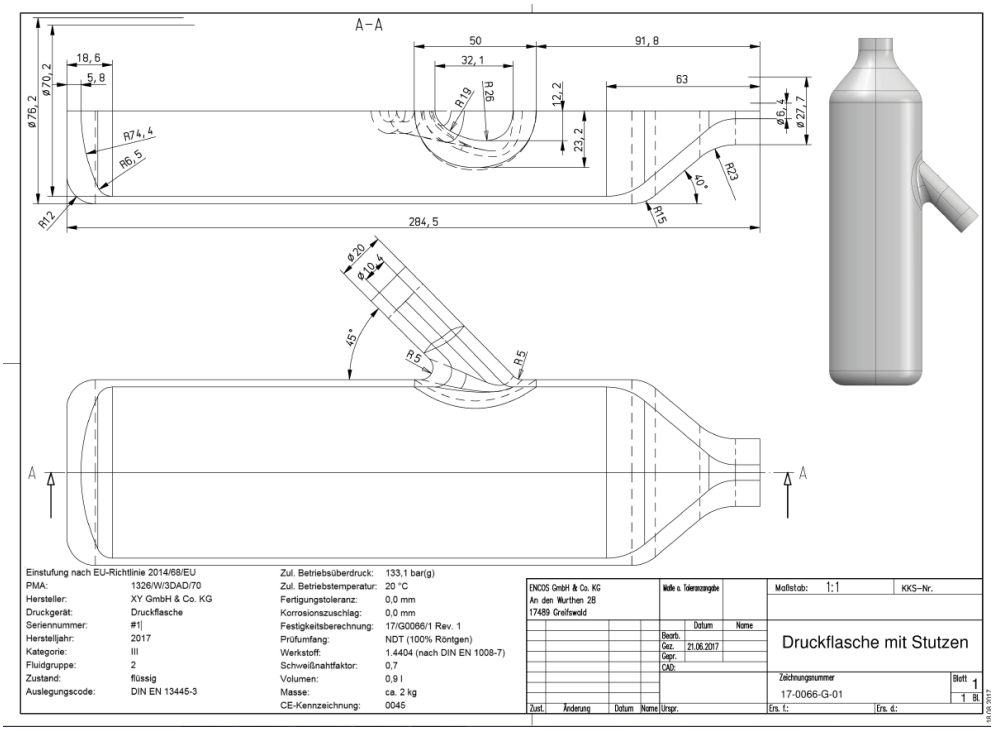

Figure 1. Construction drawing of the pressure vessel (test specimen)

The test components are constructed as a closed cylindrical body with a diameter of 76.2 mm, a flat bottom, a 45 ° (axially inclined) nozzle and a conical transition to the upper nozzle. The components were made of powder from austenitic material 1.4404 (X2 CrNiMo-17-12-2).

In a further step, the additively manufactured components, all nozzles included, were computer tomographed (CT) with the YXLON CT System "Modular" and evaluated by means of the software VolumeGraphics 3.0. The installation of the test rig and the YXLON CT "Modular" system are shown in figure 2.

Figure 2. Test specimen on CT with styrofoam housing

As a result of the defect analysis a different pore distribution and a substantial difference in the number of pores were found in both screened test specimens (see figure 3).

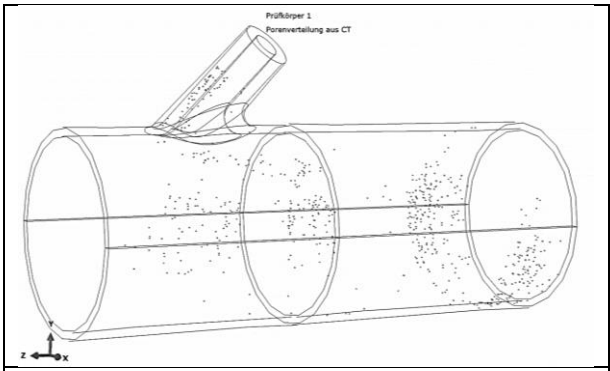

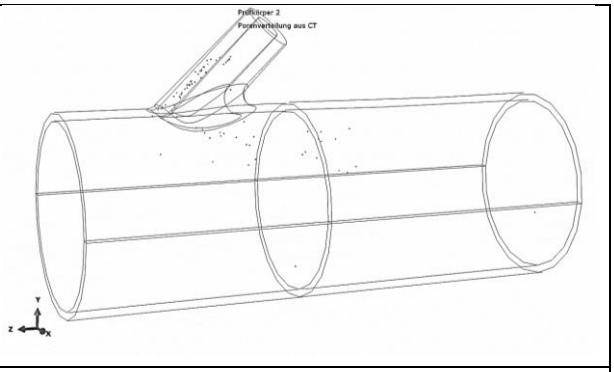

Test specimen 1		Test specimen 2	
Total number of pores	620	Total number of pores	79
Diameter of the largest pore	449 µm	Diameter of the largest pore	344 µm

Figure 3. Pore distribution in two test specimens

Furthermore, a software-supported method for pore evaluation in additively manufactured components was developed. Here, the measured pores are idealized by spheres of equal volume and then automatically subtracted from the base body. This method allows an easy meshing and subsequent calculation in established FEA software.

For the static and dynamic analyses, the following results were obtained, Schulz et al. (2018):

- The limit load analysis showed that the influence of the detected pores on the burst pressure can be neglected.
- In the case of fatigue analysis, the results show that pores act as notches in critical design areas and thus have the function of a crack initiator. Pores can significantly shorten the fatigue lifetime if they are located in areas with high stresses.
- On the other hand, it was shown in Schulz et al. (2018) that the crack growth itself is mostly independent of the presence of pores. The crack growth is accelerated slightly due to the small pore size. Approximately, the crack growth corresponds to that of a pore-free structure.

These results suggest that fatigue crack growth is very important for the evaluation of additive-fabricated components. In the case of additive manufacturing, a criterion for base-safe components should be a dampened, reduced crack growth.

EVALUATION AND INTERPRETATION OF THE RESULTS FROM FRACTURE MECHANICAL CT SAMPLES

Crack propagation behavior and microstructure of additively manufactured 316L was investigated in comparison to conventionally manufactured material. Figure 4a) displays the semi-finished test pieces, Figure 4b) the final fracture toughness specimens after electrical discharge machining. All fatigue crack growth (FCG) experiments were conducted in laboratory air at ambient temperature, applying a frequency of 20 Hz and an R-value of 0.1.

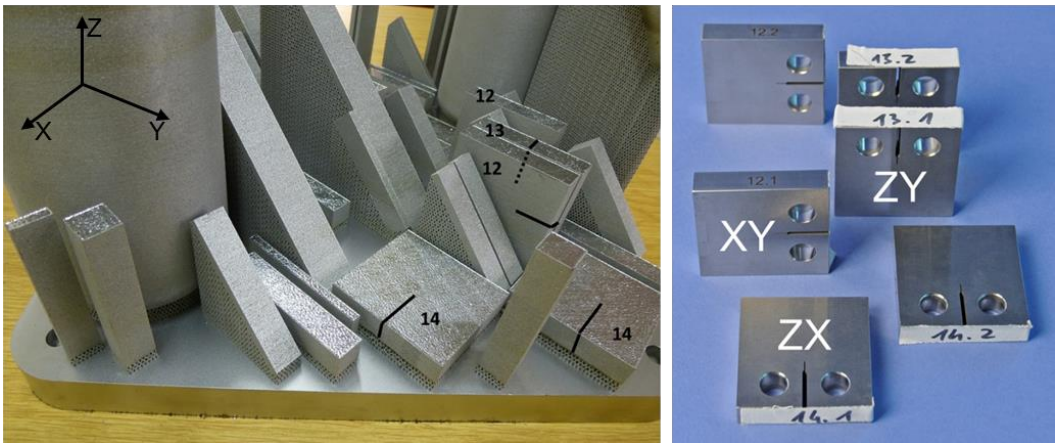

Figure 4. a) Semi-finished test pieces after SLM, b) final testing specimens (compact tension geometry).

The cyclic stress intensity factor ΔK was determined according to ASTM E647, the calculation of the cyclic crack growth rate was accomplished applying a 7-point polynomial method according to ASTM E647.

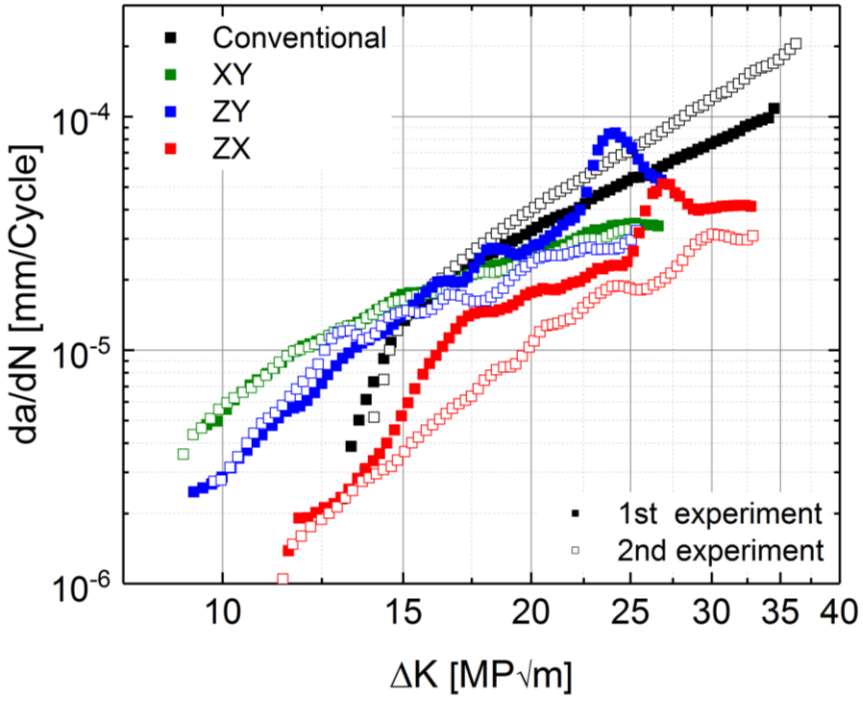

Figure 5. Crack propagation behavior of the additively manufactured specimens (SLM – Selective Laser Melting) in the different build directions compared with conventionally manufactured material

Figure 5 presents the FCG data of SLM manufactured specimens in the different build directions in comparison to conventionally manufactured material. In the XY specimen the crack path was found to propagate perpendicular to the build direction, while in ZY orientation in parallel and in ZX direction under an angle of 45° (cf. Figure 6b) and Figure 7). The crack growth rates per cycle (da/dN) of all the additively manufactured specimens were lower regardless of build direction with the only exception of a small ΔK range from ~ 23 - 26 MPa√m in case of the first ZY sample.

However, the initiation of crack propagation started at lower stress intensities than in conventional material. In the ZX specimen (crack propagation under an angle of 45° to the build direction) the lowest value of da/dN was observed accompanied by the highest ΔK (~ 11.5 MPa√m) value to initiate crack propagation of all the additively manufactured specimens. For a given value of ΔK the crack growth rates measured at the SLM material were up to 8 times lower than in the conventional material.

In contrast, an approximately 2.3 MPa√m higher ΔK value was required to initiate crack propagation in conventionally produced material. The best reproducibility was found in the XY specimens (crack path perpendicular to the build direction).

Figure 6a shows the fracture toughness specimens after fracture and figure 6b displays the crack paths in the SLM manufactured samples.

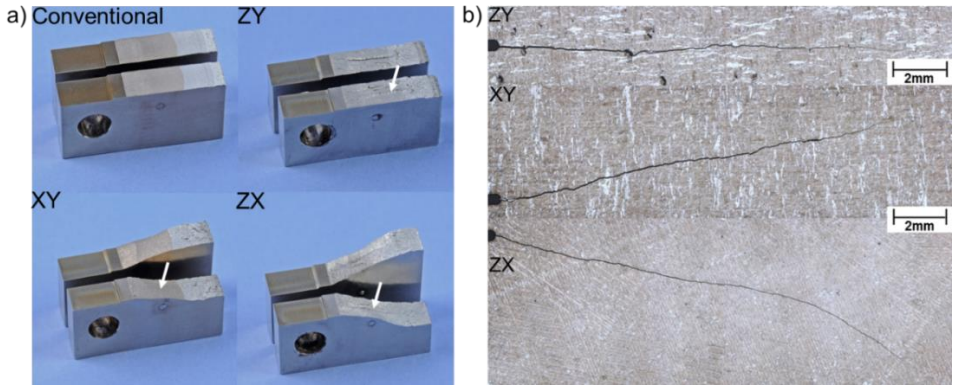

Figure 6: a) fracture toughness samples b) longitudinal crack paths in the specimens

The only specimen presenting a fracture path valid according to ASTM E647 was the one in ZY orientation. Regardless of build direction, all cracks run transcrystalline (cf. figure 6b, figure 7 and figure 9). Because of this, weak connection of the individual melt pools can be excluded as a dominant factor in cracking behavior.

Figure 7. Transcrystalline crack propagation, independent of build direction

Figure 8 shows the fracture surfaces of conventionally and SLM manufactured fracture toughness specimens. The fracture surface of the conventionally manufactured material exhibited characteristics of ductile fracture. In contrast, the XY and ZY specimens (figure 8b and c) displayed mixed fracture with ductile and cleavage areas along with several pores.

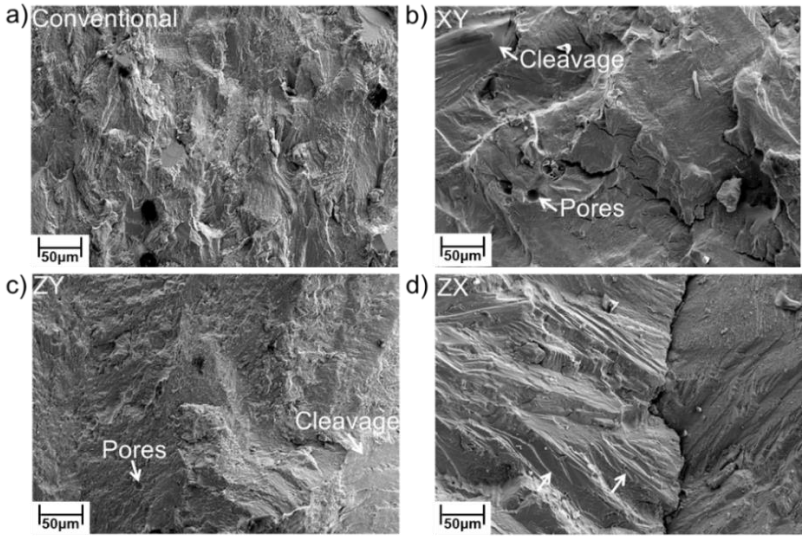

Figure 8. Fracture surfaces of a) conventionally and SLM manufactured material of build directions b) XY, c) ZY and d) ZX

The ZX (figure 8d) specimen exhibited a mixed mode fracture surface, too. It is noteworthy that the fracture path ran along lattice planes within the grains (figure 8d) and the highest percentage (13.46%) of a preferred cracking orientation {110} among all specimens was measured (figure 9) in this individual specimen.

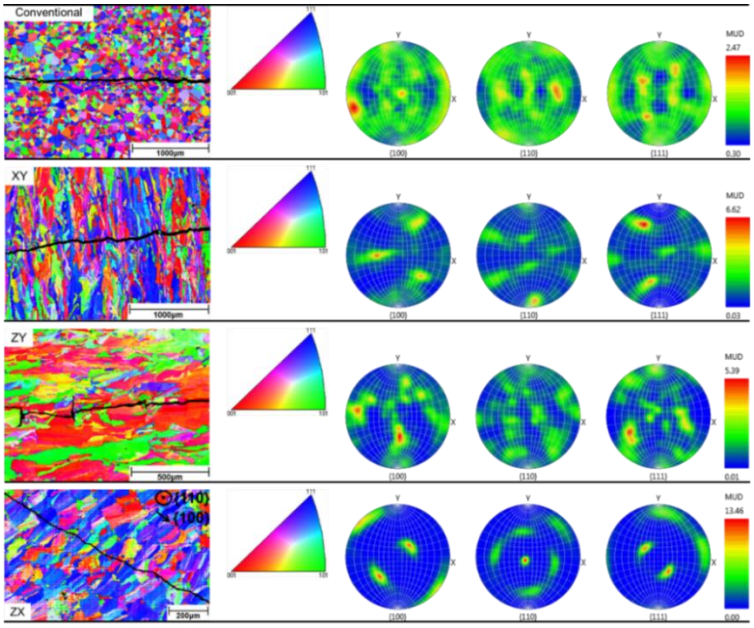

Figure 9. EBSD (Electron backscatter diffraction)-mappings (and corresponding pole figures) along fracture paths in conventionally and SLM manufactured (with regard to the 3 different build directions) materials

Furthermore, dislocations in the XY and ZX specimens were aligned perpendicular to the crack, but parallel in the ZY sample, in which the crack ran horizontally (figure 10). Depending on build direction

and the resulting orientation of grains, the occurrence of dislocations is energetically favored in certain directions, what could be a plausible explanation for the non-horizontal crack path (figure 6) in the XY and ZX specimens.

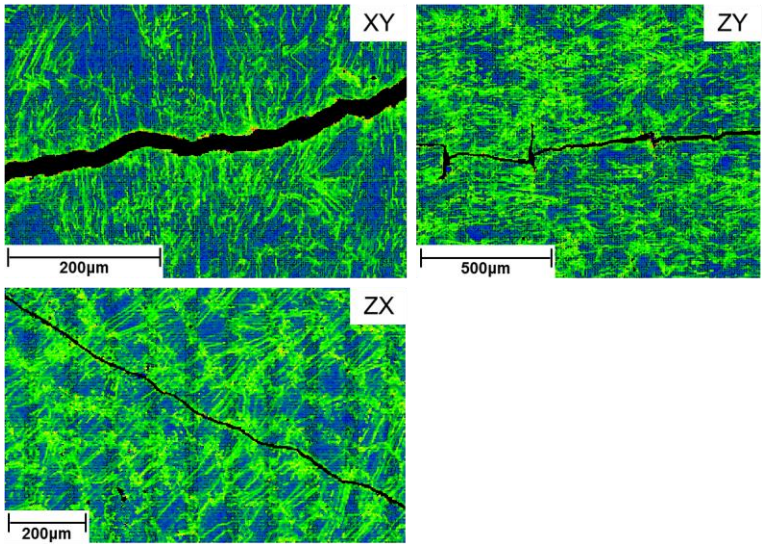

Figure 10. Local misorientation-mappings of the additively manufactured samples (with regard to the 3 different build directions)

Distribution, number and size of pores were different depending on build direction, which had direct - but limited - impact on fatigue cracking behavior. The lowest amount of small pores was observed in the ZX sample (figure 11), which also exhibited the lowest crack growth rate (figure 5). In the ZY specimen more and larger pores were observed, while in the XY sample more, but by trend smaller pores occurred. Both these specimens exhibited higher crack propagation rates (da/dN) than the ZX specimens (figure 5). It was not possible to clarify whether pores or grain orientation (resulting from build direction) were the decisive factor influencing the crack growth rate.

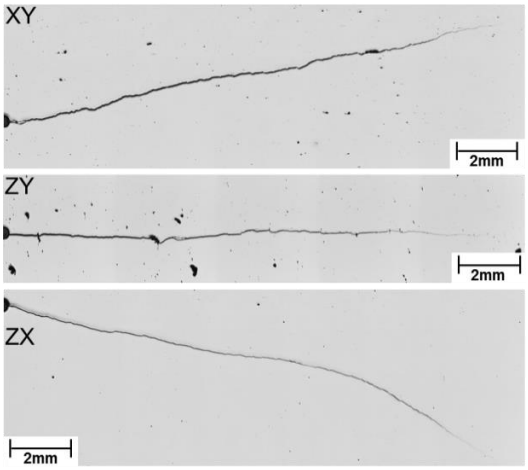

Figure 11. Exemplary number and size of pores depending on build direction

Further processing related issues, which may influence crack propagation behavior, are shown in figure 12. Finely distributed SiO_2 particles (white arrow in figure 12) were found in all the SLM

manufactured specimens. In addition, traces of segregation (figure 12 red arrow) were observed. Ni, Mo enrichment and Fe, Mn depletion were detected by energy dispersive x-ray spectroscopy (EDX) in these areas. Ni and Mo contents both directly influence solid solution hardening and consequently the strength of the material, which has a direct impact on cracking resistance and therefore on crack propagation behavior.

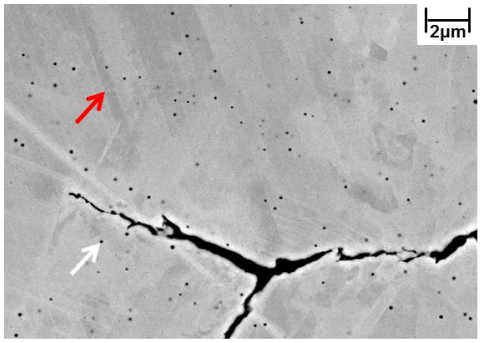

Figure 12. SiO_2-particles (white arrow) and segregation traces (red arrow)

Process optimization towards avoidance of segregation effects for this reason may offer further potential for the improvement of crack propagation resistance.

IMPORTANCE OF LOWERED CRACK PROPAGATION CURVES FOR THE COMPONENT LIFE TIME

The results of the SLM fracture toughness samples show premature crack initiation, but reduced crack growth rate (especially in the ZX specimen) compared to the conventional comparative material.

In principle, premature crack initiation does not represent a restriction of component safety. Due to the proportionality between crack initiation and the tolerable stress range, an improvement can be achieved by simple measures. For example, stress-strain ranges can be effectively reduced by optimizing the design shape of the component.

Crack growth rate is crucial for fatigue crack growth. Subsequently, it is calculated how different rates of crack growth affect crack growth and inspection intervals. This examination is carried out on the example of the stress distribution in the area of the nozzle intersection of the test component for the load case “internal pressure” (figure 14).

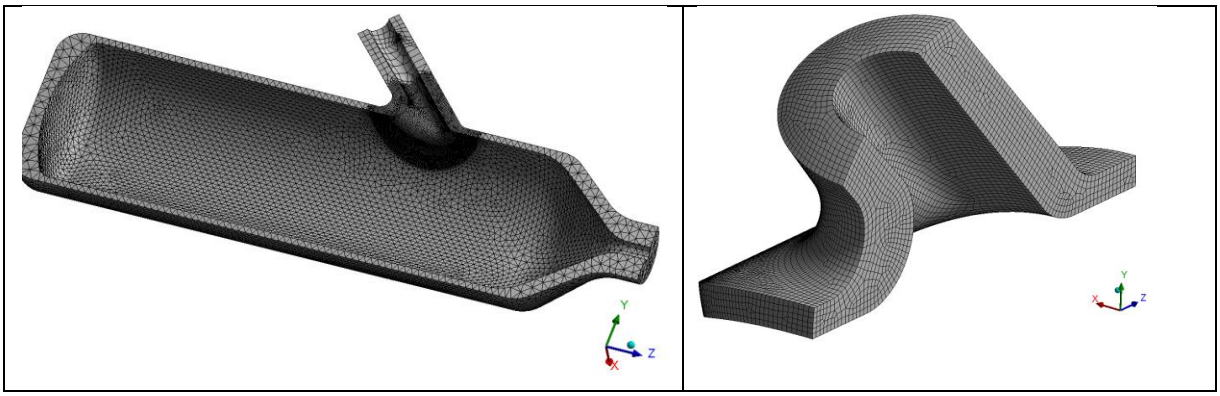

Figure 13. Test component (half model) with nozzle intersection geometry

A matrix of five different crack growth rates is examined and the influence on crack growth is compared.

Table 1: Crack growth rates matrix

Material	Austenitic steel			Ferritic steel	
Type	Conventional		Additive	Conventional	New material
Crack grow rate	ASME XI	Measured, as shown in figure 5	Measured, as shown in figure 5	ASME XI	HiperFer, See next chapter

The stress field in the nozzle intersection was calculated for an internal pressure of 133.1 bar, see figure 14.

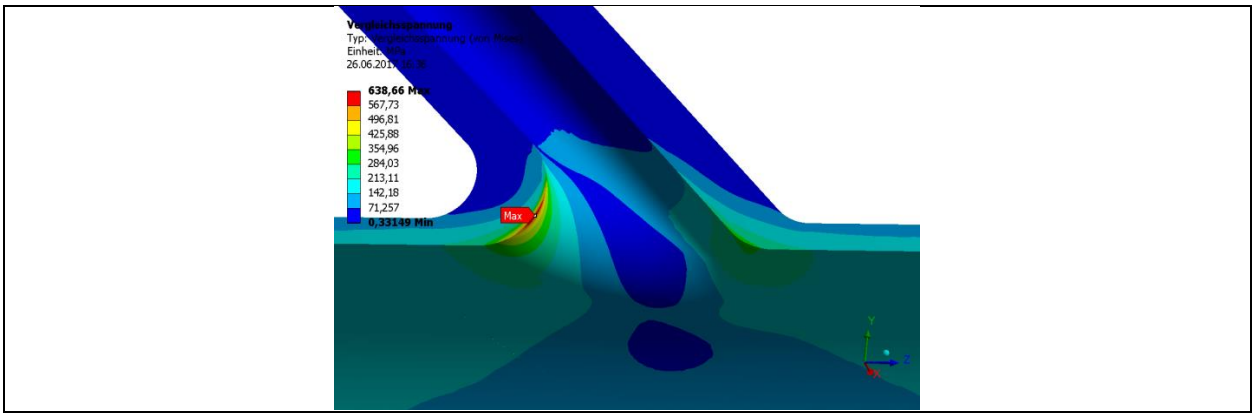

Figure 14. Stress distribution in the nozzle intersection area

For the analytical crack growth calculations, a semi-elliptical surface-crack model and the stress intensity factor solution for 2 dimensional stress fields according to Varfolomeyev et al (2000) were used. The postulated initial crack was of 2 mm crack depth and a semiaxes aspect ratio of 1/10. As cyclic loads the pressure hub between Zero and 133.1 bar acc. to Figure 14 were taken. To simulate any relevant fatigue crack growth, a scaling factor of 2 was used on these loads.

Figure 15 shows the comparison of the impact of the crack propagation rates according to Table 1 within a crack growth diagram. The results show the enormous influence of material properties (crack growth) on the component's fatigue. A further increase can be achieved here with new, optimized materials (see next chapter and the HiperFer curve in Figure 17).

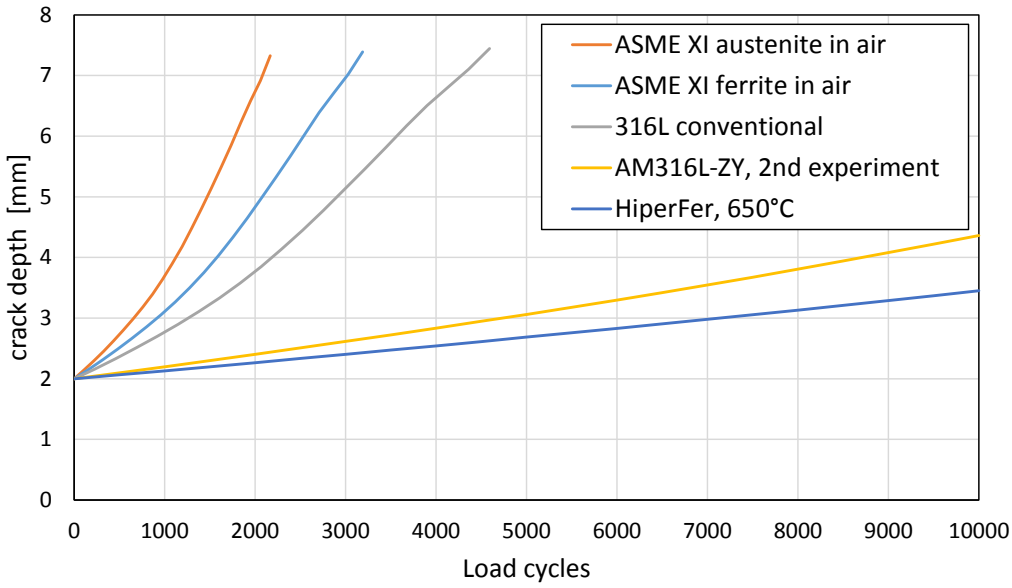

Figure 15. Crack growth diagram for a postulated 2 mm deep and 40 mm long surface crack under cyclic loads acc. to Figure 14 and different crack propagation rates listed in Table 1

PROPERTIES OF NEW MATERIALS

At this point it will be discussed the potentials can be tapped if, in the future, materials specially optimized for additive manufacturing are applied. An "AM optimized" material, which is capable to benefit from in-situ heat treatment by the so called “temper bead effect” would offer potential time and cost savings over AM processed conventional materials. A crucial prerequisite for this is rapid precipitation kinetics.

HiperFer, Kuhn and Talik (2014), a novel high chromium ferritic stainless steel, developed at Forschungszentrum Juelich, was evaluated concerning its in-situ heat treatment capability in laser metal deposition (LMD) processing. HiperFer is strengthened by a combination of solid solution and intermetallic $(Fe,Cr,Si)_2(Nb,W)$ Laves phase particle precipitation, Lopez Barrilao et al. (2016).

To (cyclic) plastic deformation at temperatures higher than 600 °C it "actively reacts" by thermomechanically induced precipitation, Kuhn et al. (2018), which contributes to an increase in component safety. By this mechanism HiperFer reaches creep and fatigue performance far beyond conventional ferritic-martensitic 9-12 Cr steels like grades 92, Kuhn et al. (2014) or X20 in combination with superior resistance to corrosion (downtime, steam oxidation and fireside). Figure 16 displays Laves phase particles, precipitated during LMD processing (accomplished by Fraunhofer ILT, Aachen) of HiperFer steel powder. The high amount of small Laves phase precipitates confirms rapid precipitation kinetics.

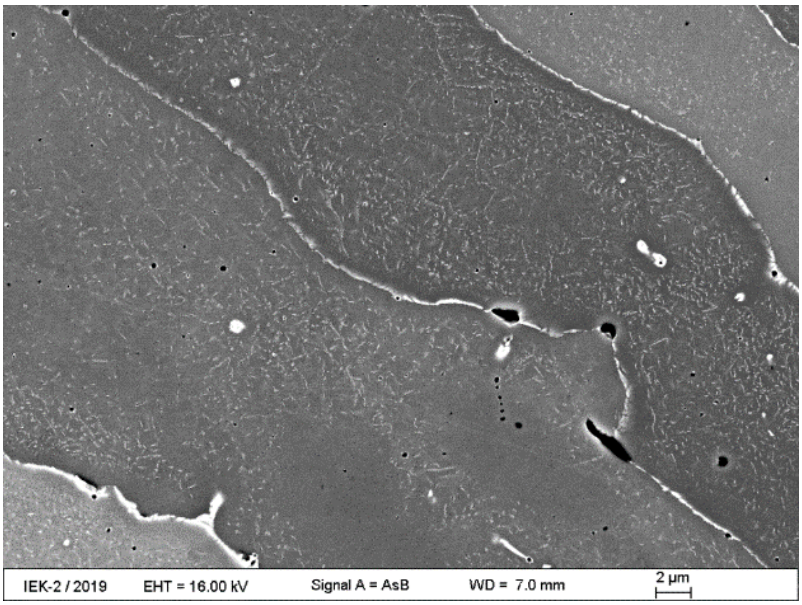

Figure 16: Laves Phase precipitates in LMD processed HiperFer steel

Several mechanisms are responsible for the improved performance of HiperFer: First, grain boundaries are occupied by Laves phase particles, what stabilizes the grain structure without embrittling the material. Second, "reactive precipitation hardening" to plastic deformation, which not only results in higher strength, but active crack obstruction and deflection (Fig. 17), Kuhn et al. (2018).

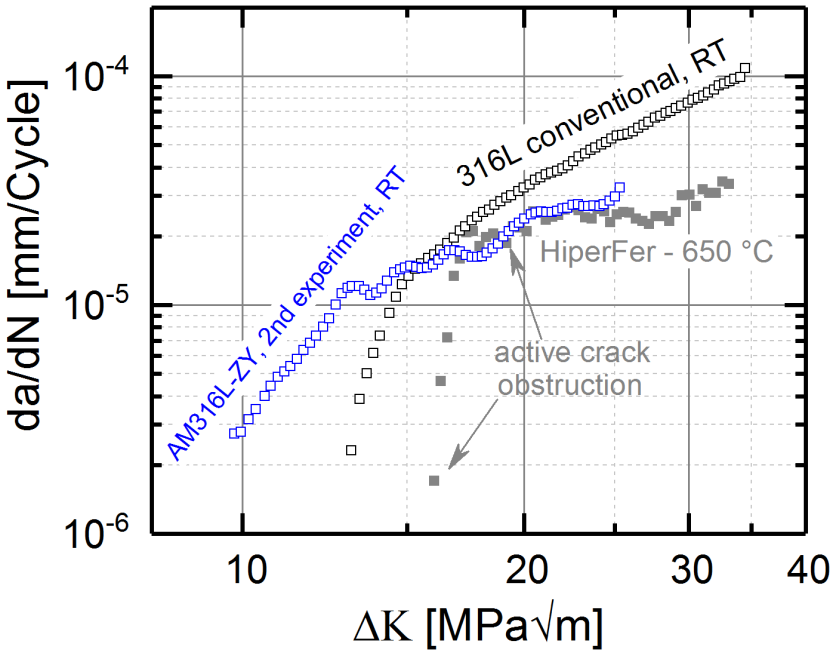

Figure 17. FCG data of AM316L and conventionally manufactured 316L at room temperature (RT) vs. HiperFer material at 650 °C (f = 20 Hz, R = 0.1)

First results of crack growth studies of conventionally manufactured HiperFer indicate that at 650 °C it reaches crack growth rates lower than in conventionally manufactured 316L and approximately equal to the AM316L at ambient temperature. It is remarkable that for the initiation of crack propagation even at 650 °C in conventionally produced HiperFer significantly higher stress intensities are required than for the conventionally and additively manufactured 316L at ambient temperature (Fig. 17). Furthermore, the crack growth rate stagnates over a comparatively wide range of stress intensities, despite of increasing ΔK values (Figure 17), which is caused by the aforementioned crack obstruction mechanisms. It can be assumed that further improvement can be achieved for an additively manufactured HiperFer.

HiperFer steel may greatly benefit from additive manufacturing techniques, because AM offers processing parameter regions, which are not accessible by conventional processing routes: HiperFer materials are predestined for in-situ heat treatment. Furthermore, material composition and build process can be mutually optimized towards, e.g. optimum in-situ tempering time and cooling rate to achieve beneficial number and size distribution of strengthening particles. Even microstructures, customized to individual loading scenarios seem feasible.

CONCLUSION

In the past, additively manufactured materials and components were often seen in connection with manufacturing defects and brittle material behavior. Fulfilling the high quality requirements in nuclear power plant construction previously seemed unthinkable. Approval procedures are still hampered by the problems of standardizing the manufacturing process.

However, the above results have shown that these problems are solvable. Common inspection methods in conjunction with modern simulation methods for static and dynamic strength analyses enable an effective evaluation of additively manufactured components with integrated pore structure.

Further potential lies in the production of materials and powders themselves. Already commercially available materials, such as the austenite investigated here, show a reduced crack growth in comparison to conventional materials. In the future, new materials such as a HiperFer will enable material properties (further reduced crack growth), which are clearly superior to conventional materials.

Thus, the high quality requirements of nuclear regulations (e.g. German codes KTA 3201 and KTA 3206, US codes ASME III and ASME XI) can also be met for additively manufactured components. A catastrophic failure of these components due to manufacturing defects does not need to be assumed, so that use of these components also in areas with a break exclusion seems possible.

REFERENCES

Schulz, A., Beckert, M., Dr. Bietke, D., Trieglaff, R., (**2018**). "Additive Manufacturing – first approaches to pore evaluation", 44th MPA-Seminar, October 17 and 18th 2018, Stuttgart.

ASME Boiler and Pressure Vessel Code, Section III (2017), Rules For Construction of Nuclear Facility Components.

ASME Boiler and Pressure Vessel Code, Section XI (2015), Rules For Inservice Inspection of Nuclear Power Plant Components.

ASTM E647-08e1, Standard test methods for measurements of fatigue crack growth rates.

KTA 3201 (2017), Components of the Reactor Coolant Pressure Boundary of Light Water Reactors

KTA 3206 (2014), Verification Analysis for Rupture Preclusion for Pressure Retaining Components in Nuclear Power Plants

Kuhn, B. and **Talik**, M. (**2014**). " HiperFer - High Performance Ferritic Steels", Proceedings of the 10th Liége Conference on Materials for Advanced Power Engineering, Liége, Belgium, P. 264 – 273; Schriften des Forschungszentrums Jülich Reihe Energie & Umwelt / Energy & Environment 234 (2014) ISBN 978-3-95806-000-5-

https://www.researchgate.net/publication/283714619_HiperFer__High_Performance_Ferritic_ Steels

Lopez Barrilao, J., Kuhn, B., Wessel, E. (**2016**). „Microstructure and Intermetallic Particle Evolution in Fully Ferritic Steels", Proceedings of the 8th International Conference on Advances in Materials Technology for Fossil Power Plants, Albufeira, Algarve, Portugal, Volume: ISBN-13: 978-1-62708-131-3, Pages 1027-1035

https://www.researchgate.net/publication/315715583_MICROSTRUCTURE_AND_INTERMETALLIC_ PARTICLE_EVOLUTION_IN_FULLY_FERRITIC_STEELS

Kuhn, B., Lopez Barrilao, J., Fischer,T., (**2018**). „Reaktive Mikrostruktur, der Schlüssel zu kostengünstigen, ermüdungsbeständigen Hochtemperaturwerkstoffen", 41. Vortragsveranstaltung FVWHT, Langzeitverhalten warmfester Stähle und Hochtemperaturwerkstoffe, Neues aus Anwendung und Forschung, 30. November 2018 Düsseldorf

Kuhn, B., Talík, M., Zurek, J., Beck, T., Quadekkers, W. J., Singheiser, L. S., (**2014**). „Development of High Chromium Ferritic Steels Strengthened by Intermetallic Phases", *Materials Science and Engineering: A* 594 (2014), pp. 372-380

Varfolomeyev, I., Gienko, A., Krasowsky, A., Schmitt, W. (**2000**), "Development of weight functions for cracks in 3D bodies", *Report T 1/2000, Fraunhofer IWM, Freiburg*